ADVANCED MATERIALS
www.advmat.de

Simultaneous Control of Spectral And Directional Emissivity with Gradient Epsilon-Near-Zero InAs Photonic Structures

*Jae S. Hwang, Jin Xu, and Aaswath P. Raman**

Controlling both the spectral bandwidth and directionality of emitted thermal radiation is a fundamental challenge in contemporary photonics. Recent work has shown that materials with a spatial gradient in the frequency range of their epsilon-near-zero (ENZ) response can support broad spectrum directionality in their emissivity, enabling high total radiance to specific angles of incidence. However, this capability is limited spectrally and directionally by the availability of materials with phonon-polariton resonances over long-wave infrared wavelengths. Here, an approach is designed and experimentally demonstrated using doped III–V semiconductors that can simultaneously tailor spectral peak, bandwidth, and directionality of infrared emissivity. InAs-based gradient ENZ photonic structures that exhibit broadband directional emission with varying spectral bandwidths and directional ranges as a function of their doping concentration profile and thickness are epitaxially grown and characterized. Due to its easy-to-fabricate geometry, it is believed that this approach provides a versatile photonic platform to dynamically control broadband spectral and directional emissivity for a range of emerging applications in heat transfer and infrared sensing.

1. Introduction

The ubiquity of thermally generated light makes its control of fundamental importance in a broad range of applications, from thermophotovoltaics[1-3] to thermal imaging[4-6] and infrared sensing.[7-9] Far-field thermal emission is typically incoherent both spatially and temporally, resulting in its broad spectrum and omnidirectional nature.[10] However, thermal emission into unwanted frequencies and directions greatly limits the efficiency of existing technologies.[11] The ability to control the spectral and angular extent of thermal emission has thus stimulated an active field of contemporary photonics and materials research.

A range of photonic strategies have been investigated to control the spectral and directional nature of thermally generated light emission, including surface plasmon polaritons,[12-17] phonon-polaritonic structures,[18-21] metasurfaces,[1,11] hyperbolic metamaterials,[22–24] and photonic crystals.[25] While significant progress has been achieved in spectrally selective thermal emitters, directional control has proven to be more challenging. When directional thermal emission has been deliberately engineered, the spectral bandwidth of directional emission is typically narrowband and the emission angle itself changes significantly as a function of wavelength. By contrast, broadband directional thermal emission control, where emissivity is highly directional to the same set of angles across a broad bandwidth, has proven to be more challenging to achieve. Recently, strategies to achieve such a capability were proposed theoretically,[26,27] and an alternate approach using polaritonic oxide-based "gradient" epsilon-near-zero (ENZ) materials was experimentally demonstrated.[28]

In gradient ENZ materials, the ENZ frequency varies spatially along a key dimension, typically the thickness of a film. Subwavelength ENZ films are known to support a leaky electromagnetic mode (the Berreman mode) near their longitudinal optical phonon frequencies in the p polarization, whose angular response is controlled by film thickness.[29-34] In recent work, gradient ENZ films were shown to support a broadband Berreman mode that in turn enabled directional thermal emission to the same angular range over 4 μm bandwidths in the long-wave infrared (LWIR) wavelength range.[28] However, a key limitation of this approach is that the gradient ENZ response was achieved using complementary phonon-polariton resonances supported by a range of oxides. This in turn meant that the spectral range, bandwidth, and directional characteristics of such thermal emitters are limited by suitable materials available in nature. Furthermore, as the resonance frequencies of the constituent layers are fixed by their intrinsic electron or phonon interactions, there is no avenue for active tuning of spectral or directional emissivity in such films.

J. S. Hwang, J. Xu, A. P. Raman
Department of Materials Science and Engineering
University of California, Los Angeles
Los Angeles, CA 90095, USA
E-mail: aaswath@ucla.edu
A. P. Raman
California NanoSystems Institute
University of California, Los Angeles
Los Angeles, CA 90095, USA

The ORCID identification number(s) for the author(s) of this article can be found under https://doi.org/10.1002/adma.202302956

DOI: 10.1002/adma.202302956

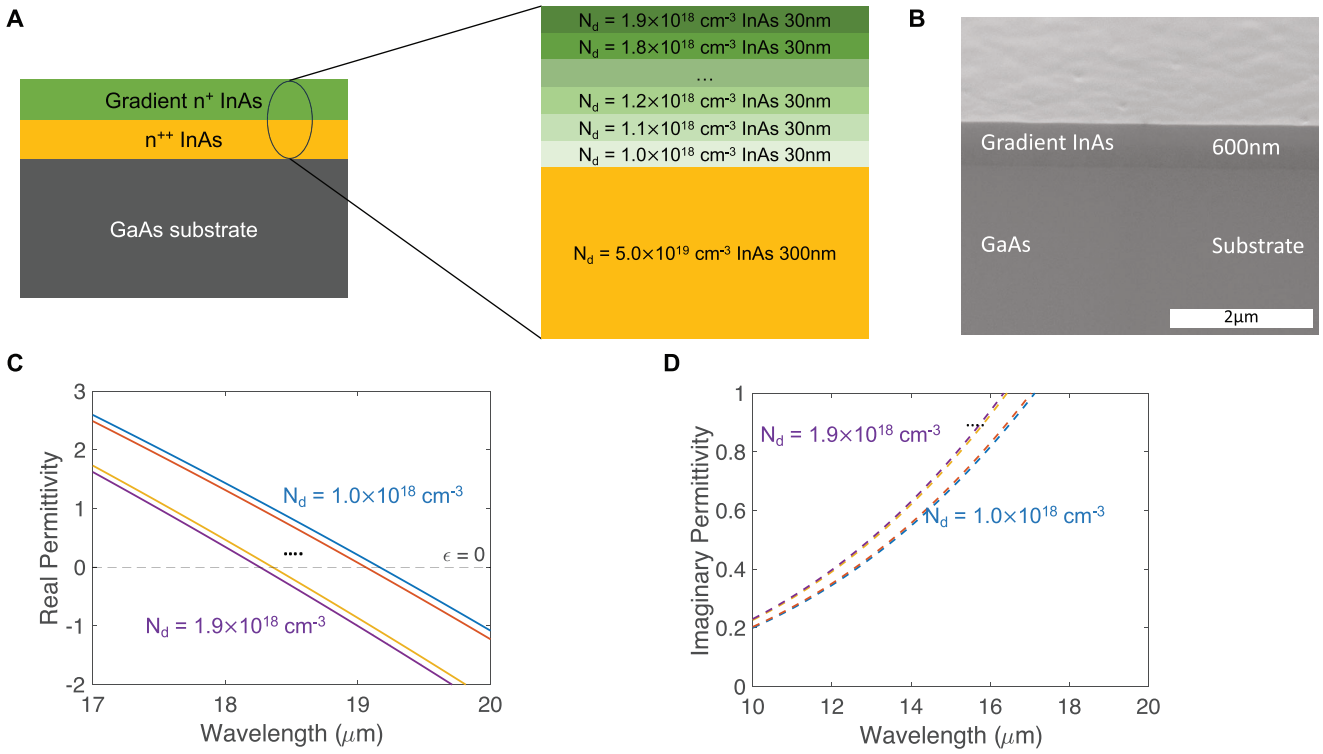

Figure 1. Configuration of an InAs-based gradient ENZ thin film for broadband directional thermal emission. A) Schematic of thermal emitter enabled by a semiconductor gradient ENZ thin film. The doping concentration of the constituent semiconductor thin films varies spatially along the depth dimension with a range from 1.9×10^{18} to 1.0×10^{18} cm^{-3}. The thickness of the individual layers is 30 nm. B) SEM image of the experimentally fabricated multilayer InAs film structure, with labels identifying the materials used and layer thicknesses. C) Numerically calculated real part of the permittivity (and the imaginary part of the permittivity (D)) of the gradient-doped semiconductor thin films with a doping concentration range from 1.9×10^{18} to 1.0×10^{18} cm^{-3}. The ENZ wavelength varies with different doping concentrations in a continuous range.

Alternatively, the desired ENZ response can be enabled by coupling to free carriers, electrons, and holes, in semiconductors. Doped semiconductors can exhibit a Drude metal-like response with their plasma frequency typically at infrared wavelengths and determined by their free carrier concentration.[35-43] Due to this capability, prior studies have used doped semiconductor-based platforms to demonstrate Tamm plasmon polariton emitters[44,45] and dynamic thermal emission control.[46-48] Broadband omnidirectional emissivity was also demonstrated using resonances supported in semiconductor nanostructures.[13,14,49] Doped semiconductors have also been used to demonstrate Berreman mode-driven behavior, including directional emission, but only over a narrow bandwidth of operation.[36,39,40] Recent work has demonstrated that multiple layers of CdO doped at different doping concentrations can yield multispectral narrowband or broadband emitters at the Brewster angle of the substrate.[50] However, past work has not demonstrated the ability to simultaneously tune the spectral bandwidth, spectral peak, and directional range of a thermal emitter. Such a capability would allow one to constrain directional emission to particular angular ranges for arbitrary spectral ranges, a challenging prospect.

Here, we present a platform for tailoring spectral and directional thermal emission with unprecedented control: semiconductor gradient ENZ photonic structures based on epitaxially grown graded doped InAs. We show that the spectral peak and bandwidth of high emissivity can be tuned to a remarkable extent by controlling both the thickness and the doping concentration profile along the depth dimension of the structure. We epitaxially grow and characterize photonic structures demonstrating, by design, high emissivity peaks between 17.5 and 19.5 μm and between 12.5 and 15 μm, respectively. Furthermore, we demonstrate directional tuning of the thermal beaming effect by controlling the total thickness of the structure, where the directionality is constant over the entire high emission bandwidth. We demonstrate directional tuning over 2 μm bandwidths from a 74° peak to a 66° peak. Our semiconductor-based platform opens up exciting possibilities for novel device concepts built on gradient ENZ materials.

2. Results

To demonstrate tailored simultaneous control of spectral and directional emissivity, we exploited the free carrier response of judiciously designed Silicon-doped InAs thin films where the doping concentration varies spatially in a graded profile along the depth dimension. The first structure we designed and grew by molecular beam epitaxy was composed of InAs thin films of the same thickness with the doping concentration ranging from 1.0×10^{18} to 1.9×10^{18} cm^{-3} (**Figure 1**A). In the first structure, the thickness of the individual layers was 30 nm each and they were epitaxially grown atop a heavily doped InAs layer with a doping concentration of 5.0×10^{19} cm^{-3} and thickness of 300 nm (Figure 1A).

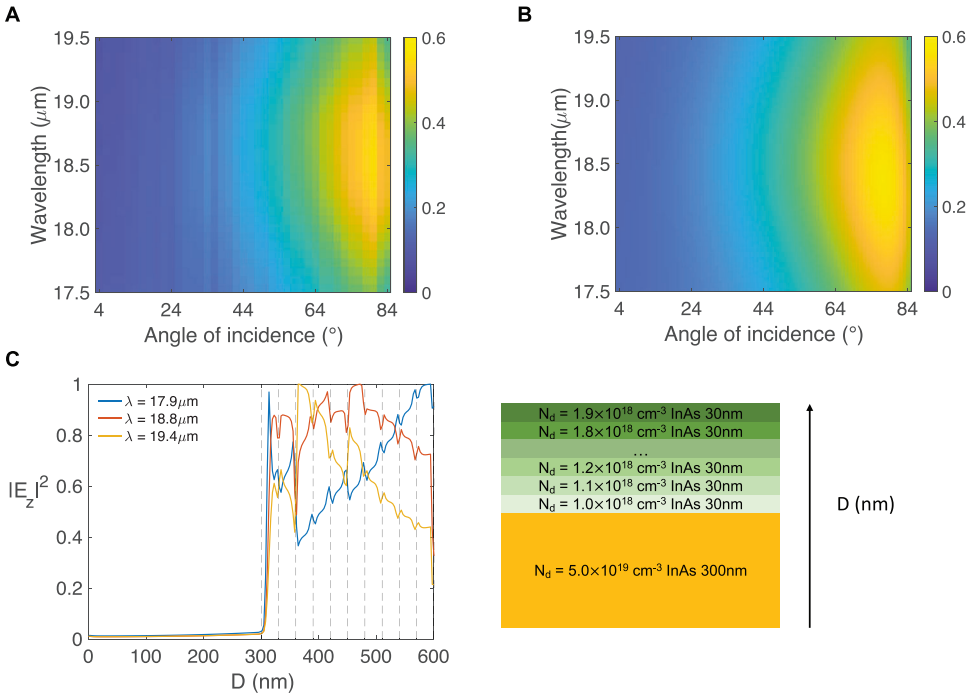

Figure 2. Comparing experimental measurements with simulated results. A) Experimentally measured emissivity spectra varying with the angle and wavelength of the fabricated multilayer semiconductor film structure in p-polarization. B) Simulation result of the emissivity spectra of the structure for p-polarization using the transfer matrix method in conjunction with a semiconductor device solver. The simulation result shows a broadband angular selective behavior in emissivity and is in good agreement with the experimental measurement. C) Simulated electric field intensity distribution for the peak emissivity angle illumination at wavelengths (λ) of 17.9, 18.8, and 19.4 μm. The layers with higher doping concentrations support the Berreman mode peak at lower wavelengths, whereas the thin films with relatively lower doping concentrations support the optical mode at higher wavelengths corresponding to their ENZ wavelengths.

The heavily doped InAs layer serves as a reflective mirror supporting the Berreman mode in the ENZ wavelength ranges of the gradient InAs thin films, as it has negative permittivity over the key wavelengths of operation of the gradient ENZ layers. The gradient ENZ InAs structure and the heavily doped InAs layer were both grown on a 50 mm (2 inch) semi-insulating GaAs substrate, with a total InAs film thickness of 600 nm (Figure 1B). We note that in these graded doped InAs layers, post-fabrication dopant diffusion is expected to be negligible based on diffusion parameters reported in the literature.[53] Furthermore, the high doping concentration range used in the gradient ENZ structures ensures that the InAs layers remain extrinsic to moderately high temperatures thereby making their spectral response largely temperature-insensitive at such temperatures (Table S2, Supporting Information).

To motivate the doping profile chosen, we show in Figure 1C,D the numerically calculated real and imaginary parts of the permittivity of the constituent semiconductor thin films of the gradient InAs layer for structure 1. We model the permittivity function of the doped InAs thin films with the Drude formalism using only the plasma wavelength and scattering time as fitting parameters. We obtain the doping-dependent plasma wavelength and scattering time values using an interpolation between the experimentally reported Drude parameters inferred from the literature[37] and validate it against our epitaxially grown reference InAs film (see Table S1 and Figure S3, Supporting Information). With increasing doping concentration from 1.0×10^{18} to 1.9×10^{18} cm^{-3}, the ENZ wavelength gradually varies from 19.2 to 18.2 μm (Figure 1C) while the permittivity of the heavily doped (n^{++} InAs) layer remains highly negative in this wavelength range, allowing the field to be locally confined in the gradient ENZ layer. Due to their complementary resonance frequencies that vary gradually along the depth dimension, layering these semiconductor thin films will result in a III–V-based gradient ENZ thin film where its broadband spectral emission is more continuous and tunable, compared to the previously demonstrated gradient ENZ thin films based on polaritonic oxides.[28]

We show in **Figure 2**A the emissivity spectra of the fabricated structure varying with angle and wavelength in the p-polarization, as measured by an FTIR spectrometer. Since our structures were deposited on an optically thick metal layer, the transmissivity (T) is equal to 0 and the emissivity (ϵ) is determined through the measured reflectivity (R) as a function of polar angle of incidence ($\epsilon = 1 - R$). The obtained spectrum exhibits a strong high emissivity resonance band spanning continuously along the wavelength range from 18.2 to 19.2 μm associated with the ENZ wavelength range of the constituent semiconductor thin films of the gradient ENZ film. The emissivity spectra also show a strong angularly selective behavior in which the high emission angular range, where the overall p-polarized emissivity is above 0.4 throughout the 17.5–19.5 μm range, is centered at 76° (Figure 2A). The dispersion relation of this optical mode is calculated in Figure S2 (Supporting Information), showing a broadband Berreman mode supported to the left of the light line.

To further validate our experimental results, we next show the simulated emissivity spectra calculated using the transfer matrix method in conjunction with a semiconductor device solver (Figure 2B). The semiconductor device solver calculates the spatial distribution of the free carrier concentration in the gradient ENZ structures by self-consistently solving Poisson's equation and the drift-diffusion equations based on the finite element method. Here, we account for the Fermi-level alignment between the graded doped InAs layers, thereby accurately modeling the spectral emissivity arising from the homojunctions of the gradient ENZ layer in our simulations, as shown in Figure S6 (Supporting Information). In the optical simulation using the transfer matrix method, as in our experiments, we assume by Kirchhoff's law that the emissivity is equal to the absorptivity, and calculate it as $\epsilon = 1 - R$. The simulation results agree well with the experimental results, with both exhibiting strong directional emissivity throughout a broad bandwidth between 17.5 and 19.5 μm. In terms of directional characteristics, the angular range of high emissivity and peak angle of incidence also agree well with the experimental data.

To elucidate the origin of this behavior in our structures, we calculated the electric field intensity distribution for the peak emissivity angle illumination at wavelengths (λ) of 17.9, 18.8, and 19.4 μm in the p-polarization (Figure 2C). The constituent layers of the gradient ENZ thin film with higher doping concentrations support the Berreman mode at shorter wavelengths ($\lambda \approx 17.9$ μm) within the high emissivity spectral bandwidth. Thus, the field intensity profile shows larger field enhancement localized at the upper layers at these wavelengths. We note that the lowest ENZ layer also has high field intensity at 17.5 μm due to the Fermi-level alignment between the graded doped InAs layer and the heavily doped InAs reflector (Figure S7, Supporting Information). The layers with relatively lower doping concentrations support the optical mode at longer wavelengths ($\lambda \approx 19.4$ μm) and the field intensity profile shows a larger field enhancement localized at the lower layers at these wavelengths. At wavelengths near the peak emission ($\lambda \approx 18.8$ μm), the field is enhanced throughout the gradient ENZ layer. This localized field enhancement can be easily understood by considering two adjacent media, 1 and 2, characterized by a permittivity of ϵ_1, ϵ_2 and electric field of E_1, E_2, respectively. The z-component of electric displacement field $\mathbf{D} = \epsilon\mathbf{E}$ is continuous at the interface of the two adjacent mediums so that $E_{z,2} = (\epsilon_1/\epsilon_2)\ E_{z,1}$.[29] It follows that the field $E_{z,2}$ is enhanced if ϵ_2 approaches zero near the ENZ wavelength of medium 2 (Figure 1C). We also note that the heavily doped InAs layer remains highly reflective over the wavelength ranges of operation, exhibiting close to zero electric field intensity in the simulations. In principle, the peak emissivity can be enhanced by either increasing the thickness or doping concentration of the heavily doped (n^{++} InAs) layer (Figure S8, Supporting Information). Both methods allow the InAs reflector to further suppress any optical power leaking toward the bottom of the emitter.

We next show that III–V semiconductor-based gradient ENZ materials enable exceptional control of the spectral range and bandwidth of high emissivity by controlling the doping concentration gradient of the gradient ENZ thin film. We fabricated a second semiconductor gradient ENZ structure (structure 2) with the doping concentration of the gradient ENZ thin film ranging from 2.0×10^{18} to 4.5×10^{18} cm^{-3}. We note that this structure has both a different range as well as a larger spatial gradient of the doping concentration compared to structure 1, from which we expected to both change the peak spectral position to shorter wavelengths and increase the overall bandwidth of high emissivity. The thickness of the individual layers was 50 nm so the overall total thickness of the gradient ENZ thin film was 300 nm, identical to structure 1. We measured the emissivity spectra varying with the angle and wavelength of the fabricated multilayer semiconductor film structure in the p-polarization (**Figure 3**A). We observe high emissivity in the wavelength range from 12.5 to 15 μm corresponding to the ENZ wavelength range of the constituent semiconductor thin films of the gradient ENZ layer (Figure S1, Supporting Information). The emissivity spectra also show a strong directional behavior in which the angular range of high emissivity, where the overall p-polarized emissivity is above 0.4 throughout the 12.5–15 μm range, is centered at 74° (Figure 3A), similar to structure 1, but over a different and wider spectral range.

As with structure 1, we compared the experimental results against simulations using the transfer matrix method and saw excellent agreement, with both simulations and experiments exhibiting angular regions of high and low emissivity throughout a broad bandwidth between 12.5 and 15 μm. The operational range as well as the angles of operation and peak angle of incidence agree well with the experimental data (Figure 3B). To better characterize the tunability of the spectral range and bandwidth of operation, we plotted the spectral emissivity at peak emissivity angles for both structures 1 and 2 (**Figure 4**). We clearly see that the two structures exhibit different operation ranges corresponding to the ENZ wavelength range of the constituent layers of the gradient ENZ film. We also observe that the operational bandwidth of structure 2 is wider than structure 1 due to the larger spatial gradient of its doping concentration. This highlights the remarkable control over spectral emissivity bandwidth that III–V-based gradient ENZ structures can provide by controlling the doping concentration profile of the gradient ENZ layer. Other ENZ materials based on phonon-polariton resonances could partially overlap with the spectral range of the InAs-based photonic structures in the present work in terms of their resonance frequencies.[54] However, a key limitation of using phonon resonances lies in not being able to achieve complementary resonance frequencies that vary gradually and continuously along the depth dimension for arbitrary spectral ranges. Additionally, when using a phonon-polariton-based approach, the imaginary part of the permittivity can vary significantly from layer to layer, resulting in varying directional ranges of high emissivity. A doped semiconductor approach, as we demonstrate here, allows us to arbitrarily tune both the bandwidth and spectral range by carefully tuning the graded doping profile of the gradient ENZ layers while maintaining a nearly identical imaginary part of the permittivity through each layer. Such a tailored degree of control is not achievable with a phonon-polariton-based approach. Furthermore, we note that among III–V semiconductors, InAs can theoretically support a large electron dopant density up to 1×10^{20} cm^{-3}, due to its unusually high Fermi level stabilization point.[55] This thus allows one to, in principle, tune the InAs-based gradient ENZ platform over a very wide spectral bandwidth.

We next demonstrate that, in addition to tuning the spectral bandwidth, one can simultaneously tune the directional response

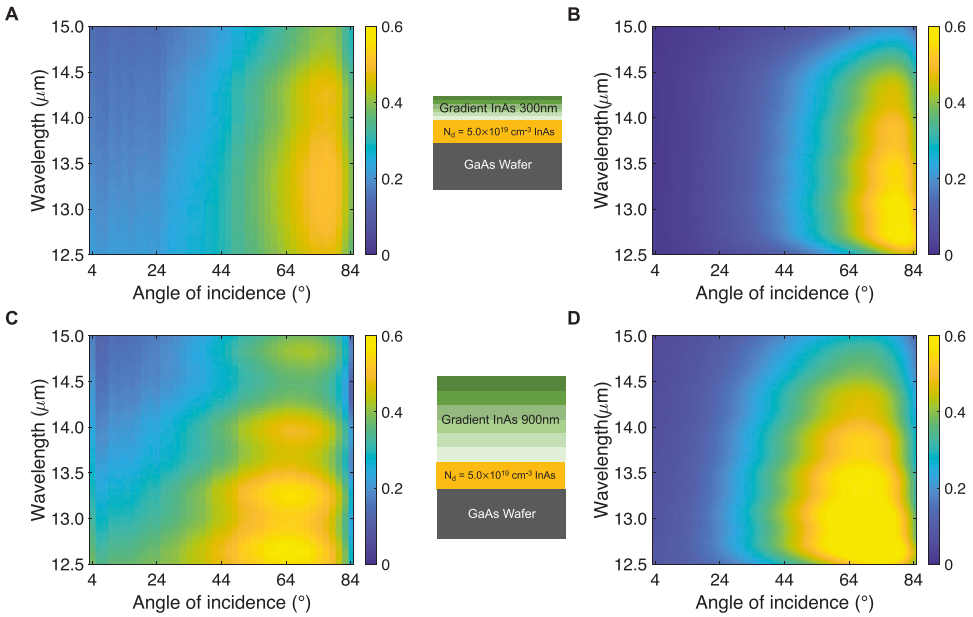

Figure 3. Tuning the directionality of the broadband directional thermal emitter by controlling the total thickness of the semiconductor gradient ENZ thin film. A,C) Measured emissivity spectra varying with angle and wavelength of the two fabricated multilayer semiconductor film structures in p-polarization with the same doping concentration range from 2.0×10^{18} to 4.5×10^{18} cm^{-3}, but different total thickness of 300 and 900 nm. B,D) Simulation results of the emissivity spectra of the structures for p-polarization using the transfer matrix method. The simulation results are in good agreement with the experimental measurements.

of semiconductor thin film-based gradient ENZ materials by controlling the total thickness of the gradient ENZ layer. We fabricate an additional gradient ENZ structure (structure 3) with the doping concentration range of the gradient ENZ thin film ranging from 2.0×10^{18} to 4.5×10^{18} cm^{-3}, identical to structure 2. Here, the thickness of the individual layers was increased to 150 nm so that the total thickness of the gradient ENZ thin film was 900 nm. For structure 3, the emissivity spectrum exhibits high emissivity in the same wavelength range as structure 2 (from 12.5 to 15 μm) (Figure 3C), corresponding to the ENZ wavelengths of the constituent semiconductor thin films of the gradient ENZ layers. The emissivity spectra show a strong, broadband directional response. However, the directional peak, where the overall p-polarized emissivity is above 0.4 throughout the 12.5–15 μm range, was centered at 66° (Figure 3C). The simulation result using the transfer matrix method also shows a similar shift in the peak emission angle toward normal incidence as compared to structure 2 (Figure 3B,D). For structure 2, we measured an average emissivity of >0.4 in the p-polarization over the wavelength range of operation (from 12.5 to 15 μm) between 66° and 80° (**Figure 5**A, red line). Outside of this angular range, the average emissivity drops below 0.3 at 50°.

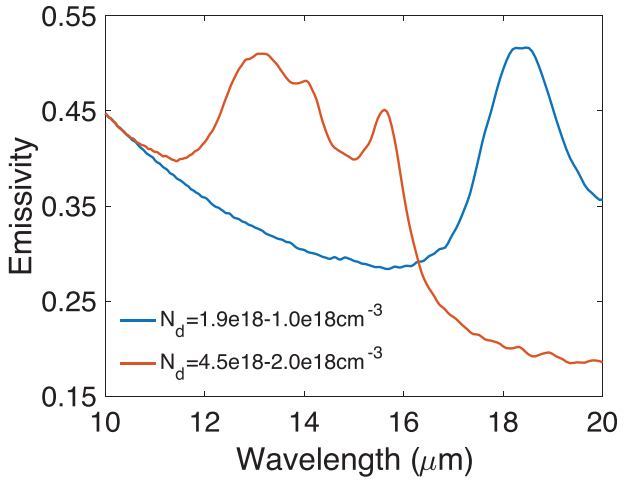

Figure 4. Tuning the spectral peak and bandwidth of the broadband directional thermal emitter by controlling the doping concentration profile of the gradient ENZ layer. Comparison of the measured emissivity in p-polarization between the two gradient ENZ structures with different doping concentration ranges at a 76° angle of incidence. The working range of structure 2 is situated at lower wavelengths and the bandwidth is wider compared to structure 1.

For structure 3, over the same wavelength range of operation (from 12.5 to 15 μm) for p-polarization, we instead observe an average emissivity >0.4 between 58° and 74° (Figure 5A, black line). Outside of this angular range, the average emissivity drops to below 0.3 at 40°. By controlling the doping concentration gradient and thickness, we are thus able to achieve exquisite and tailored control over the directional range of high emissivity while maintaining that directional response over a broad bandwidth by design. As is seen in Figure 5B, this response originates fundamentally from the spatial shift of the optical mode supported by the thicker gradient ENZ InAs photonic structure relative to the thinner one. As the total thickness of the gradient ENZ layer increases, the dispersion curve of the broadband Berreman mode moves to the left and thus will couple to modes from angles of incidence that are closer to normal incidence, agreeing well with

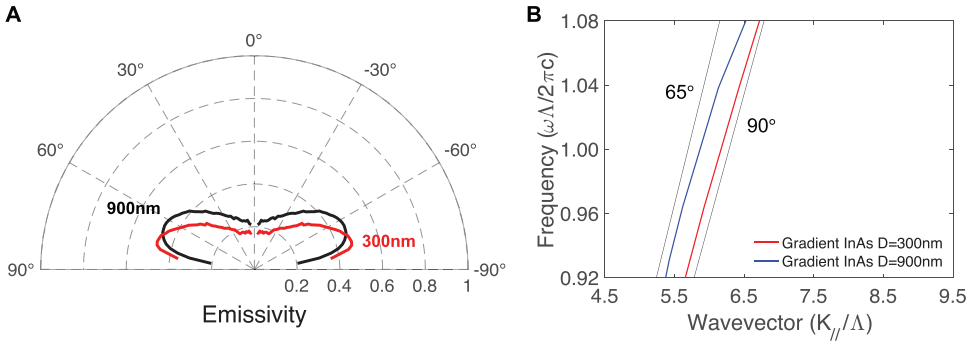

Figure 5. Directional response of the two gradient ENZ thin films with different total thicknesses. A) Polar plot of the measured average emissivity over a broad wavelength range of operation (from 12.5 to 15 μm) varying with the angle of incidence for p-polarization in structures 2 and 3, with peak emissivity observed at 74° and 66°, respectively. The larger total thickness of the gradient ENZ thin film shifts the high emissivity angle toward normal incidence. B) The calculated dispersion relation of structures 2 and 3 throughout the frequency range of interest. The broadband Berreman mode moves toward normal incidence as the total thickness of the gradient ENZ layer increases from 300 to 900 nm, which agrees with (A) (where Λ, a scaling factor, is the mean of the wavelength range of operation).

Figure 5A. In the ideal gradient ENZ framework, the spectral range of operation and directional response of a gradient ENZ film can be tuned arbitrarily and simultaneously without affecting the angular width of high emissivity (Figure S4, Supporting Information). In real materials, however, we note that the imaginary part of the permittivity can place limits on the directional contrast of emissivity. If the imaginary part of the permittivity is large for the constituent ENZ films at wavelengths near the ENZ wavelength, high emissivity will occur over a wide range of k values, and thus broader range of angles, especially for gradient ENZ films with larger total thicknesses designed to operate at near-normal angles of incidence. However, in a III–V-based gradient ENZ platform, the imaginary part of the permittivity varies gradually, but only minimally along the depth dimension for the constituent ENZ films at these wavelength ranges (Figure 1C,D; Figure S1, Supporting Information), enabling broadband spectral emission that is highly directional compared to the gradient ENZ structures based on phonon-polariton resonances, where the variability in the imaginary permittivity near the ENZ wavelengths can be substantial.

We also calculate the electric field intensity distribution for the peak emissivity angle illumination at 12.6, 13.4, and 14.5 μm using electromagnetic simulations in both polarizations for structures 2 and 3 (Figures S9 and S10, Supporting Information), where the localized field enhancement can be understood by the same argument as previously discussed for structure 1. Although the enabled directional control is in the p-polarization, it also enables a marked contrast in the polarization-averaged thermal emission as a function of angle because the emissivity is minimal at all angles in the s-polarization over the spectral operational range (Figure S5, Supporting Information). This capability not only makes our approach immediately useful for applications in heat signature control, but also in the realm of free-space optical sensing and communication,[51] by virtue of its polarization-sensitive response.

Alternative materials systems such as graphene or other 2D materials have also been investigated for their potential use in thermal emission control[56-58] and optical modulation[59-61] since their carrier density and hence their complex refractive index can be tuned by chemical doping or electrostatic gating.[62] However, the directional controllability of the broadband Berreman mode, we have demonstrated, necessitates significantly thicker films (micrometer-scale) than conventional 2D material demonstrations, thus their utilization for spectral and directional control of thermal emission remains a topic for further investigation. We believe that with the versatility of controlling both the spectral and directional optical response, the demonstrated III–V semiconductor-based photonic structures could be harnessed for a range of applications such as infrared photodetection[63,64] and light modulation[65,66] for optical communication, as well as for optical switches and logic gates in photonic integrated circuits.[67,68]

3. Conclusion

We have demonstrated a III–V semiconductor-based platform that offers unprecedented control of spectral and directional emissivity over infrared wavelengths. We show that our gradient ENZ scheme has the capability to tune the spectral bandwidth and spectral range of operation of a directional emitter arbitrarily and simultaneously. Furthermore, by controlling the total thickness of the gradient ENZ structure, we show that the angular response can be independently tuned as well. We emphasize that in our approach a directional emitter has emissivity that is highly directional to the same set of angles, across an arbitrary bandwidth. By constraining directional emission to particular angular ranges over arbitrary spectral ranges, improved performance may be possible for a range of applications, including thermophotovoltaics,[69] radiative cooling,[70] and waste heat recovery.[71] It is noteworthy that the lithography/patterning-free, chip-scale geometry, we have used, suggests that the semiconductor gradient ENZ structures can be incorporated with other photonic structures, opening up exciting possibilities for leveraging the broad spectrum modes supported by gradient ENZ structures. Since the optical response of the semiconductor gradient ENZ photonic structures is driven by free carrier concentration, these properties can be dynamically controlled,[35] potentially over the broadband operational wavelength range of directional thermal emission,[48] as well as broadband non-reciprocal thermal emission control.[51,52] We thus believe that this approach

holds great potential to enable on-demand control of broadband directional thermal emission.

Supporting Information

Supporting Information is available from the Wiley Online Library or from the author.

Acknowledgements

J.S.H. and J.X. contributed equally to this work. The authors thank Komron Shayegan and Harry Atwater, as well as Kaicheng Pan and Mark Goorsky for experimental assistance. This material was based upon work supported by the National Science Foundation under grant no. ECCS-2146577, the DARPA Young Faculty Award (#W911NF2110345) and the Sloan Research Fellowship (Alfred P. Sloan Foundation).

Note: Figure 3 and 4 were reversed on initial publication online. This was corrected while the article was in Early View.

Conflict of Interest

The authors declare no conflict of interest.

Data Availability Statement

The data that support the findings of this study are available from the corresponding author upon reasonable request.

Keywords

doped semiconductors, nanophotonics, plasmonics, thermal emission, gradient ENZ materials, broadband

Received: March 30, 2023
Revised: July 5, 2023
Published online: August 9, 2023

[1] J. Mason, S. Smith, D. Wasserman, *Appl. Phys. Lett.* **2011**, *98*, 241105.
[2] D. Jung, S. Bank, M. L. Lee, D. Wasserman, *J. Opt.* **2017**, *19*, 123001.
[3] E. Sakr, P. Bermel, *Opt. Express* **2017**, *25*, A880.
[4] M. Vollmer, in *Computer Vision: A Reference Guide*, Springer, Berlin, Germany **2021**, pp. 666–70.
[5] G. C. Hulley, R. M. Duren, F. M. Hopkins, S. J. Hook, N. Vance, P. Guillevic, W. R. Johnson, B. T. Eng, J. M. Mihaly, V. M. Jovanovic, S. L. Chazanoff, Z. K. Staniszewski, L.e Kuai, J. Worden, C. Frankenberg, G. Rivera, A. D. Aubrey, C. E. Miller, N. K. Malakar, J. M. Sánchez Tomás, K. T. Holmes, *Atmos. Meas. Tech.* **2016**, *9*, 2393.
[6] E. Lucchi, *Renewable Sustainable Energy Rev.* **2018**, *82*, 3077.
[7] Z. Pan, Y. Zhang, Z. Cheng, J. Tong, Q. Chen, J. Zhang, J. Zhang, X. Li, Y. Li, *Sensors* **2017**, *17*, 473.
[8] Y. Gong, S. S. Oh, D. L. Huffaker, N. Copner, Frontiers in Optics / Laser Science, OSA Technical Digest, Optical Society of America, Washington, DC **2018**, https://doi.org/10.1364/FIO.2018.JTu3A.89.
[9] L. Palchetti, G. Di Natale, G. Bianchini, *J. Geophys. Res.* **2016**, *121*, 10804.
[10] D. G. Baranov, Y. Xiao, I. A. Nechepurenko, A. Krasnok, A. Alù, M. A. Kats, *Nat. Mater.* **2019**, *18*, 920.
[11] D. Costantini, A. Lefebvre, A. L. Coutrot, I. Moldovan-Doyen, J. P. Hugonin, S. Boutami, F. Marquier, H. Benisty, J. J. Greffet, *Phys. Rev. Appl.* **2015**, *4*, 014023.
[12] P. J. Hesketh, J. N. Zemel, B. Gebhart, *Phys. Rev. B* **1988**, *37*, 10803.
[13] S. Law, C. Roberts, T. Kilpatrick, L. Yu, T. Ribaudo, E. A. Shaner, V. Podolskiy, D. Wasserman, *Phys. Rev. Lett.* **2014**, *112*, 017401.
[14] S. Wang, Y. Wang, S. Zhang, W. Zheng, *Phys. Lett. A* **2017**, *381*, 1439.
[15] B. Kong, V. Sokolov, K. Kim, R. Trew, *J. Appl. Phys.* **2008**, *103*, 056101.
[16] F. B. Barho, F. Gonzalez-Posada, L. Cerutti, T. Taliercio, *Adv. Opt. Mater.* **2020**, *8*, 1901502.
[17] J. R. Nolen, A. Cleri, K. Kelley, E. L. Runnerstrom, J. Nordlander, T. G. Folland, J. P. Maria, J. D. Caldwell, *Adv. Photonics Res.* **2022**, *3*, 2200146.
[18] J. J. Greffet, R. Carminati, K. Joulain, J. P. Mulet, S. Mainguy, Y. Chen, *Nature* **2002**, *416*, 61.
[19] G. Lu, M. Tadjer, J. D. Caldwell, T. G. Folland, *Appl. Phys. Lett.* **2021**, *118*, 141102.
[20] Z. Sakotic, A. Krasnok, N. Cselyuszka, N. Jankovic, A. Alú, *Phys. Rev. Appl.* **2020**, *13*, 064073.
[21] R. Duggan, Y. Ra'di, A. Alù, *ACS Photonics* **2019**, *6*, 2949.
[22] S. Campione, F. Marquier, J. P. Hugonin, A. R. Ellis, J. F. Klem, M. B. Sinclair, T. S. Luk, *Sci. Rep.* **2016**, *6*, 34746.
[23] S. Campione, T. S. Luk, S. Liu, M. B. Sinclair, *Opt. Mater. Express* **2015**, *5*, 2385.
[24] S. Molesky, C. J. Dewalt, Z. Jacob, *Opt. Express* **2013**, *21*, A96.
[25] M. Laroche, C. Arnold, F. Marquier, R. Carminati, J. J. Greffet, S. Collin, N. Bardou, J. L. Pelouard, *Opt. Lett.* **2005**, *30*, 2623.
[26] C. Argyropoulos, K. Q. Le, N. Mattiucci, G. D'aguanno, A. Alù, *Phys. Rev. B* **2013**, *87*, 205112.
[27] G. Barbillon, E. Sakat, J. P. Hugonin, S. A. Biehs, P. Ben-Abdallah, *Opt. Express* **2017**, *25*, 23356.
[28] J. Xu, J. Mandal, A. P. Raman, *Science* **2021**, *372*, 393.
[29] S. Vassant, J. P. Hugonin, F. Marquier, J. J. Greffet, *Opt. Express* **2012**, *20*, 23971.
[30] J. Rensberg, Y. Zhou, S. Richter, C. Wan, S. Zhang, P. Schöppe, R. Schmidt-Grund, S. Ramanathan, F. Capasso, M. A. Kats, C. Ronning, *Phys. Rev. Appl.* **2017**, *8*, 014009.
[31] J. Yoon, M. Zhou, M. A. Badsha, T. Y. Kim, Y. C. Jun, C. K. Hwangbo, *Sci. Rep.* **2015**, *5*, 12788.
[32] T. Shaykhutdinov, A. Furchner, J. Rappich, K. Hinrichs, *Opt. Mater. Express* **2017**, *7*, 3706.
[33] Md. A. Badsha, Y. C. Jun, C. K. Hwangbo, *Opt. Commun.* **2014**, *332*, 206.
[34] J. M. Ane, M. Huetz-Aubert, *Int. J. Thermophys.* **1986**, *7*, 1191.
[35] A. Boltasseva, H. A. Atwater, *Science* **2011**, *331*, 290.
[36] T. Taliercio, V. N. Guilengui, L. Cerutti, E. Tournié, J. J. Greffet, *Opt. Express* **2014**, *22*, 24294.
[37] S. Law, D. C. Adams, A. M. Taylor, D. Wasserman, *Opt. Express* **2012**, *20*, 12155.
[38] Y. B. Li, R. A. Stradling, T. Knight, J. R. Birch, R. H. Thomas, C. C. Phillips, I. T. Ferguson, *Semicond. Sci. Technol.* **1993**, *8*, 101.
[39] Y. C. Jun, T. S. Luk, A. Robert Ellis, J. F. Klem, I. Brener, *Appl. Phys. Lett.* **2014**, *105*, 131109.
[40] A. Cleri, J. Tomko, K. Quiambao-Tomko, M. V. Imperatore, Y. Zhu, J. R. Nolen, J. Nordlander, J. D. Caldwell, Z. Mao, N. C. Giebink, K. P. Kelley, E. L. Runnerstrom, P. E. Hopkins, J. P. Maria, *Phys. Rev. Mater.* **2021**, *5*, 035202.
[41] G. V. Naik, V. M. Shalaev, A. Boltasseva, *Adv. Mater.* **2013**, *25*, 3264.
[42] R. T. Holm, J. W. Gibson, E. D. Palik, *J. Appl. Phys.* **1977**, *48*, 212.
[43] M. Fehrenbacher, S. Winnerl, H. Schneider, J. Döring, S. C. Kehr, L. M. Eng, Y. Huo, O. G. Schmidt, K. Yao, Y. Liu, M. Helm, *Nano Lett.* **2015**, *15*, 1057.

[44] M. He, J. R. Nolen, J. Nordlander, A. Cleri, N. S. Mcilwaine, Y. Tang, G. Lu, T. G. Folland, B. A. Landman, J. P. Maria, J. D. Caldwell, *Nat. Mater.* **2021**, *20*, 1663.
[45] M. Kaliteevski, I. Iorsh, S. Brand, R. A. Abram, J. M. Chamberlain, A. V. Kavokin, I. A. Shelykh, *Phys. Rev. B* **2007**, *76*, 165415.
[46] J. Park, J. H. Kang, X. Liu, S. J. Maddox, K. Tang, P. C. Mcintyre, S. R. Bank, M. L. Brongersma, *Sci. Adv.* **2018**, *4*, eaat3163.
[47] Z. Dong, R. K. Vinnakota, A. F. Briggs, L. Nordin, S. R. Bank, D. A. Genov, D. Wasserman, *J. Appl. Phys.* **2019**, *126*, 043101.
[48] S. Vassant, I. Moldovan Doyen, F. Marquier, F. Pardo, U. Gennser, A. Cavanna, J. L. Pelouard, J. J. Greffet, *Appl. Phys. Lett.* **2013**, *102*, 081125.
[49] K. Aydin, V. E. Ferry, R. M. Briggs, H. A. Atwater, *Nat. Commun.* **2011**, *2*, 517.
[50] K. P. Kelley, E. L. Runnerstrom, E. Sachet, C. T. Shelton, E. D. Grimley, A. Klump, J. M. Lebeau, Z. Sitar, J. Y. Suen, W. J. Padilla, J. P. Maria, *ACS Photonics* **2019**, *6*, 1139.
[51] K. Shayegan, B. Zhao, Y. Kim, S. Fan, H. Atwater, Sci. Adv. **2022**, 18, eabm4308.
[52] Z. Zhang, L. Zhu, *Phys. Rev. Appl.* **2023**, *19*, 014013.
[53] E. F. Schubert, J. B. Stark, T. H. Chiu, B. Tell, *Appl. Phys. Lett.* **1988**, *53*, 293.
[54] N. Kinsey, C. Devault, A. Boltasseva, V. M. Shalaev, *Nat. Rev. Mater.* **2019**, *4*, 742.
[55] E. Tokumitsu, *Jpn. J. Appl. Phys.* **1990**, *29*, L698.
[56] K. Ito, H. Iizuka, *J. Appl. Phys.* **2016**, *120*, 163105.
[57] M. Freitag, H. Y. Chiu, M. Steiner, V. Perebeinos, P. Avouris, *Nat. Nanotechnol.* **2010**, *5*, 497.
[58] R. J. Shiue, Y. Gao, C. Tan, C. Peng, J. Zheng, D. K. Efetov, Y. D. Kim, J. Hone, D. Englund, *Nat. Commun.* **2019**, *10*, 109.
[59] T. Mueller, F. Xia, P. Avouris, *Nat. Photonics* **2010**, *4*, 297.
[60] M. Liu, X. Yin, E. Ulin-Avila, B. Geng, T. Zentgraf, L. Ju, F. Wang, X. Zhang, *Nature* **2011**, *474*, 64.
[61] A. Vakil, N. Engheta, *Science* **2011**, *332*, 1291.
[62] A. Elbanna, H. Jiang, Q. Fu, J. F. Zhu, Y. Liu, M. Zhao, D. Liu, S. Lai, X. W. Chua, J. Pan, Z.e X. Shen, L. Wu, Z. Liu, C. W. Qiu, J. Teng, *ACS Nano* **2023**, *17*, 4134.
[63] L. Nordin, A. Kamboj, P. Petluru, E. Shaner, D. Wasserman, *ACS Photonics* **2020**, *7*, 1950.
[64] L. Nordin, P. Petluru, A. Kamboj, A. J. Muhowski, D. Wasserman, *Optica* **2021**, *8*, 1545.
[65] J. Park, B. G. Jeong, S. I.l Kim, D. Lee, J. Kim, C. Shin, C. B. Lee, T. Otsuka, J. Kyoung, S. Kim, K. Y. Yang, Y. Y. Park, J. Lee, I. Hwang, J. Jang, S. H. Song, M. L. Brongersma, K. Ha, S. W. Hwang, H. Choo, B. L. Choi, *Nat. Nanotechnol.* **2021**, *16*, 69.
[66] P. P. Iyer, M. Pendharkar, C. J. Palmstrøm, J. A. Schuller, *ACS Photonics* **2019**, *6*, 1345.
[67] M. Fetterman, C. P. Chao, S. R. Forrest, *IEEE Photonics Technol. Lett.* **1996**, *8*, 69.
[68] J. E. Zucker, K. L. Jones, B. I. Miller, U. Koren, *IEEE Photonics Technol. Lett.* **1990**, *2*, 32.
[69] N. Horiuchi, *Nat. Photonics* **2020**, *14*, 66.
[70] A. P. Raman, M. A. Anoma, L. Zhu, E. Rephaeli, S. Fan, *Nature* **2014**, *515*, 540.
[71] P. S. Davids, J. Kirsch, A. Starbuck, R. Jarecki, J. Shank, D. Peters, *Science* **2020**, *367*, 1341.